Hindawi
Advances in Civil Engineering
Volume 2019, Article ID 2031520, 10 pages
https://doi.org/10.1155/2019/2031520

*Research Article*

# Study on Bending Damage Constitutive Model and Mechanical Properties of Limestone Based on Acoustic Emission

**Yuanshuai Zhang**,[1] **Shuangying Zuo**,[1] **Bo Yu**,[2] **Shiwan Chen**,[1] **and Jienan Jia**[3]

[1]*College of Resource and Environmental Engineering, Guizhou University, Guiyang 550025, China*
[2]*Power China Guiyang Engineering Corporation Limited, Guiyang 550081, China*
[3]*CCCC Highway Consultants Co., Ltd., Guizhou Branch, Guiyang 550003, China*

Correspondence should be addressed to Shuangying Zuo; syzuo@gzu.edu.cn

Received 2 August 2019; Revised 25 September 2019; Accepted 1 October 2019; Published 30 October 2019

Academic Editor: Chun-Qing Li

Copyright © 2019 Yuanshuai Zhang et al. This is an open access article distributed under the Creative Commons Attribution License, which permits unrestricted use, distribution, and reproduction in any medium, provided the original work is properly cited.

To reveal the mechanical characteristics and damage evolution mechanism of limestone in the bending process, the cumulative acoustic emission (AE) hits were used to define the damage variable, and the rock microbody hypothesis and the Weibull distribution function were applied to further improve the damage variable. Meanwhile, the bending damage constitutive model of limestone under three-point bending was developed based on the Lemaitre strain equivalence principle and the continuum damage theory. Then, the three-point bending test with acoustic emission monitoring was carried out to verify the rationality and validity of the model. Results showed that the modified damage variable $D$ had an exponential distribution with the strain $\varepsilon$, and the damage was mainly concentrated in the macrocrack propagation stage. Moreover, the bending neutral layer moved towards the compressive zone in the bending damage process. The bending neutral layer, furthermore, moved slowly a small distance at the initial stage of bending fracture but moved fast a long distance at the end stage of bending fracture. In addition, the bending damage constitutive model could be quantitatively expressed by the cumulative AE hits $N_p$, the stress $\sigma$, the strain $\varepsilon$, and Young's modulus $E$. The theoretical stress-strain model curves agreed well with experimental results, which demonstrated that the proposed model could capture the damage evolution of limestone reasonably in the bending process.

## 1. Introduction

The compressive strength of rock has received many attentions due to the conception that rock is usually under a compressive loading condition [1]. However, the stability of rock structures may be dominated by bending tensile stresses in many environments [2–5], which is a major hidden danger, possibly causing a serious engineering accident in a sudden occasion. For instance, there may be a slide-bending failure in the bedding rock slope, a crooked-toppling failure in the antidip layered rock slope, and a buckling failure in the vertical rock slope [6]. Besides, the bending, collapse, and bulge of the surrounding rock in underground engineering relate to the bending tensile stress [7]. Because of its great engineering significance, some studies on bending tensile stress have been proposed. The direct tension test was first applied to determine the tensile strength of rock [8]. Then, ASTM and ISRM [9, 10] developed the Brazilian test, an indirect method for determining rock tensile strength. Additionally, Pandey and Singh [11] studied another indirect method, three-point bending test (TPBT). Gradually, some stress-strain constitutive models were proposed, the continuum damage theory of rock was accepted, and the acoustic emission (AE) monitoring technique was applied.

The concentrations of the existed studies show that the three-point bending test, a widely used indirect method in studying the tensile stress during rock bending, and the acoustic emission (AE) monitoring technique, a reliable nondestructive testing method for analyzing rock failure characteristics [12–14], have been applied to study rock damage. Yao et al. [15] systematically studied the effects of loading rate and preload on the dynamic bending failure of

Laurentian granite. Prem and Murthy [16] applied AE technique to study the damage mechanism of the reinforced concrete beams under bending and classified the damage in the beams into four zones. Lacidogna et al. [17] examined the stress-dependent damage progress in prenotched concrete beams tested in bending by the AE and dynamic identification techniques. Lu et al. [18] conducted a series of three-point bending tests on sandstone beam specimens with type I precracks to study the microcracks and microscopic deformation behavior of samples during real-time loading. Kaklis et al. [19] focused on the investigation of the three-point bending tensile strength of Dionysos marble and compared the calculated bending tensile strength with the corresponding value obtained from Brazilian indirect tension as well as ring tests. Zhang et al. [20] studied the damage and fracture process of three-point bending notched sandstone beams by combining the three-point bending test together with the digital image correlation (DIC) and acoustic emission (AE) techniques. Yao et al. [21] proposed a two-parameter tensile strength model for rocks based on the successful application of the nonlocal theory and the three-point bending test. Rong et al. [22] studied the effects of initial thermal cracking on the physical and mechanical behavior of coarse marble using uniaxial compression test and acoustic emission test. Chen et al. [23] conducted a series of acoustic emission compression tests on rock samples to study the damage evolution characteristics of rock during loading. Jin et al. [24] confirmed the highly positive correlation between the plastic strain of the loaded coal and the AE characteristic parameters through the AE test during coal uniaxial compression.

Previous studies have focused on the qualitative analysis of rock deformation and failure process, and some progress has been made. However, few studies have been conducted on relations among the damage variable, the stress, the strain, and the cumulative AE hits. In this paper, the research focus is to derive the bending damage constitutive model of limestone based on the Lemaitre strain equivalence principle, the continuum damage theory, and the material mechanics. Meanwhile, the three-point bending test with acoustic emission monitoring was also carried out to verify the rationality and validity of the model. And the mechanical characteristics and damage evolution mechanism of limestone in the bending process were analyzed finally. The results may be helpful for the understanding of the fracturing mechanism of limestone and provide some guidelines for field applications [25].

## 2. A Bending Damage Model Based on AE

*2.1. Hypothesis of the Bending Damage Model.* According to the previous studies on the bending damage of concrete and rock [26–28], the following basic assumptions are originally stated in the process of deriving the bending constitutive model:

(a) The bending damage meets the Lemaitre strain equivalence principle

(b) The bending damage conforms to material mechanics assumptions such as continuous, small deformation, and flat section

(c) The bending damage distributed only in the tensile zone but not in the compressive zone

*2.2. Damage Evolution and Constitutive Relation of the Tensile Zone.* The stress-strain constitutive relationship of the tensile zone in the bending damage process can be expressed as equation (1) based on the continuum damage theory and the Lemaitre strain equivalence principle [29, 30].

$$\sigma_t = E(1 - D)\varepsilon, \tag{1}$$

where $\varepsilon$ is the strain, $\sigma_t$ is the tensile stress, $E$ is Young's modulus, and $D$ is the damage variable.

According to Tang's study [31], the relationship between the damage variable and the cumulative AE hits can be directly defined as

$$D = \frac{N}{N_m}, \tag{2}$$

where $N$ is the cumulative AE hits in the bending damage process and $N_m$ is the cumulative AE hits in completely damaged rock.

According to Wu's study [32], when the rock exhibits brittle behavior, the relationship between the cumulative AE hits over testing time can be described by the following equation:

$$N = A_1 \exp(Bt) + C, \tag{3}$$

where $A_1$, $B$, and $C$ can be determined by testing data.

In the above equation (2), it is hard to obtain the cumulative AE hits $N_m$ because the test machine usually stops working before the rock is completely damaged. Therefore, this paper replaces $N_m$ with $N_p$ and amends equation (2) as

$$D = K\frac{N}{N_p}, \tag{4}$$

where $N_p$ is the cumulative AE hits at the end of test and $K$ is the assumed correction coefficient.

Substituting equation (3) into equation (4), equation (5) can be derived:

$$D = K \cdot \frac{A_1 \exp(Bt) + C}{N_p}. \tag{5}$$

To determine the correction coefficient $K$ in equation (5), the rock microbody hypothesis has been taken as the theoretical basis, assuming that the microelement strength is conformed to the Weibull distribution [31, 33, 34]. Then, the damage evolution equation can be derived as

$$m = \frac{1}{\ln\left(E\varepsilon_p/\sigma_p\right)}, \tag{6}$$

$$D = 1 - \exp\left[-\frac{1}{m}\left(\frac{\varepsilon}{\varepsilon_p}\right)^m\right], \tag{7}$$

where $m$ is the Weibull modulus, which determines the shape of the distribution, $\varepsilon_p$ is the tensile strain at the end of the test, and $\sigma_p$ is the tensile stress at the end of test.

Assuming the damage variable of testing final failure is $D_p$, then substitute $D_p$, $N_p$, $\varepsilon_p$, and $m$ into equations (4)–(7). Finally, the damage variable correction coefficient $K$ can be derived as equation (8):

$$K = 1 - \frac{\sigma_p}{E\varepsilon_p}. \tag{8}$$

Through the simultaneous solution of equations (4), (5), and (8), the evolution equation of the damage variable with testing time based on acoustic emission is finally derived as

$$D = \left(1 - \frac{\sigma_p}{E\varepsilon_p}\right)\frac{A_1 \exp(Bt) + C}{N_p}. \tag{9}$$

In continuum damage theory and material mechanics, when there is a displacement-controlled mechanical test, the strain evolution with testing time obeys the following equation:

$$\varepsilon = A_2 t, \tag{10}$$

where $A_2$ can be determined by testing data.

The relationship of the damage variable with strain evolution can be derived by substituting equation (10) into equation (9).

$$D = \left(1 - \frac{\sigma_p}{E\varepsilon_p}\right)\frac{A_1 \exp\left((B/A_2)\varepsilon\right) + C}{N_p}. \tag{11}$$

Substituting equations (9) and (10) into equation (1), the evolution equation of tensile stress with testing time is derived as

$$\sigma_t = E\left\{1 - \left[\left(1 - \frac{\sigma_p}{E\varepsilon_p}\right)\frac{A_1 \exp(Bt) + C}{N_p}\right]\right\}(A_2 t). \tag{12}$$

Subtracting the testing time from equations (9) and (10) and then substituting the result into equation (1), the stress-strain relationship in the bending deformation process can be derived as

$$\sigma_t = E\left\{1 - \left[\left(1 - \frac{\sigma_p}{E\varepsilon_p}\right)\frac{A_1 \exp\left((B/A_2)\varepsilon\right) + C}{N_p}\right]\right\}\varepsilon. \tag{13}$$

*2.3. Damage Evolution and Constitutive Relation of the Compressive Zone.* In this study, the stress-strain constitutive relation of the limestone bending compressive zone can be derived without considering the damage in the bending process as

$$\sigma_c = E\varepsilon, \tag{14}$$

where $\sigma_c$ is the compressive stress.

According to equations (10) and (14), the evolution equation of compressive stress with testing time in the bending region of limestone can be derived as

$$\sigma_c = EA_2 t. \tag{15}$$

*2.4. Space-Time Evolution Equation of the Bending Neutral Layer.* According to scholars' research, bending damage will degrade the mechanical properties of rocks, reduce the bearing capacity, weaken the bending stiffness, and move the neutral layer towards the compressive zone [35–37]. Consequently, it is one of the important contents to study the movement of the neutral layer in the bending process.

A schematic diagram of the bending force of the cross section of the limestone is shown in Figure 1. In Figure 1, $y_0$ is the distance that the neutral layer moves to the compressive zone at a certain testing time $t$, $Z$ is the initial position of the neutral layer, and $Z'$ is the position after the neutral axis moves. Where, the positive direction of the $y$-axis refers to the direction of bending and tension.

From the basic theory of material mechanics, the relationship between the strain and the neutral layer distance can be derived as

$$\varepsilon = \frac{y}{\rho}, \tag{16}$$

where $\rho$ is the radius of curvature and $y$ is the distance from a certain position to the bending neutral layer.

Taking the new bending neutral layer $Z'$ as a reference, the axial force equation of limestone during bending deformation can be derived as

$$N = \int_{-(h/2)+y_0}^{0} \sigma_c \cdot b \cdot \mathrm{d}y + \int_{0}^{h/2+y_0} \sigma_t \cdot b \cdot \mathrm{d}y. \tag{17}$$

The axial force along the length of the specimen is zero because of the force on the vertical section of the specimen during bending:

$$N = 0. \tag{18}$$

Solving equations (1), (14), and (16)–(18), the following equation can be derived:

$$\left(y_0 - \frac{h}{2}\right)^2 - (1 - D)\left(\frac{h}{2} + y_0\right)^2 = 0. \tag{19}$$

Substituting equation (9) into equation (19) and simplifying it, the space-time evolution equation of the bending neutral layer can be derived as

$$y_0 = \frac{h\left(1 - \sqrt{1 - \left(1 - \left(\sigma_p/E\varepsilon_p\right)\right)\left(\left(A_1 \exp(Bt) + C\right)/N_p\right)}\right)}{2 + 2 \cdot \sqrt{1 - \left(1 - \left(\sigma_p/E\varepsilon_p\right)\right)\left(\left(A_1 \exp(Bt) + C\right)/N_p\right)}}. \tag{20}$$

## 3. Model Validation and Discussion

*3.1. Three-Point Bending Test with AE Monitoring.* To verify the rationality and effectiveness of the above-mentioned bending damage model, tests were conducted on six limestone samples having $L = 600$ mm and square cross section of side 100 mm as shown in Figure 2. The testing equipment used in the test included WAW-1000 kN microcomputer controlled electro-hydraulic servo universal testing machine (Figure 3(a)), DH3818 static strain data acquisition instrument (Figure 3(b)),

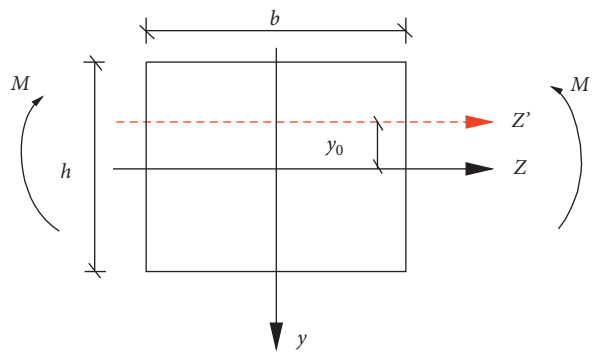


Figure 1: A schematic diagram of the bending force of the cross section of the limestone.

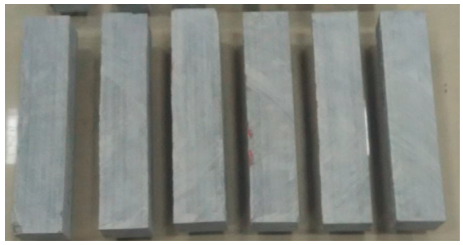

Figure 2: The limestone sample geometry.

and the PCI-2 type acoustic emission system (Figure 3(c)). To explain the test more intuitively, the three-point bending loading configuration and strain gauge layout are shown in Figure 4, the installed limestone sample is shown in Figure 5(a), and the fractured limestone sample is shown in Figure 5(b). The test operation steps are as follows:

(1) The surface of the limestone sample was polished by fine sandpaper.

(2) The strain gauges were coupled to the side and bottom of the limestone samples. Where, strain gauge 3 was located at the bending neutral layer position, strain gauges 1 to 5 were separated by 15 mm, and strain gauge 6 was located at the bottom of the samples.

(3) The limestone sample with the strain gauges was connected to the DH3818 static strain data acquisition instrument. Meanwhile, a standby limestone sample was also connected to compensate the temperature of the test.

(4) The AE probes were fixed at the front and rear sides of the limestone sample with a rubber band.

(5) The parameters of loading and AE were preset. Here, the controlled displacement increased continuously with a velocity of 0.002 mm/s, the AE monitoring threshold was 45 dB, the timing parameter PDT was 50 $\mu$s, the HDT was 200 $\mu$s, the HLT was 300 $\mu$s, the acquisition frequency was 1MSPS, and the preamplifier gain was 40 dB.

(6) The limestone sample was tested, up to final failure, AE signals were recorded, and loading test data were acquired, too.

*3.2. Basic Parameters of the Bending Damage Model.* Fit equation (3) to get the basic parameters $A_1$, $B$, and $C$. Meanwhile, fit equation (10) to get the basic parameter $A_2$. The fitting curve between theory equations with testing data is shown in Figures 6 and 7. The parameter fitting values of $A_1$, $B$, and $C$ are listed in Table 1. The parameter fitting values of $A_2$ are listed in Table 2. Also, the basic physical parameter values of the limestone are listed in Table 3.

*3.3. Verification and Discussion of the Bending Damage Variable.* Substituting the parameters of Tables 1–3 into equations (9) and (11), the evolution equation of the damage variable with testing time can be derived as equation (21) and the evolution equation of the damage variable with the strain can be derived as in Table 4.

$$D = 1.72157 \times 10^{-10} \times e^{0.29t}. \tag{21}$$

Substitute the bending testing time $t$ into equation (21) and the strain $\varepsilon$ into Table 4. The evolution curve of damage variables is shown in Figure 8.

According to the analysis of Figure 8, the damage variable $D$ tended to 0 in the range of 0 s–65 s but increased rapidly in the macrocrack propagation process (in the range of 65 s–80 s), which showed that the limestone exhibited an elastic-brittle behavior in the bending process. That is, the limestone suffered from an instantaneous bending failure without plastic deformation features, and the damage was mainly concentrated in the unstable macrocrack growth stage. In addition, as can be seen from Figure 8, the modified damage variable $D$ had an exponential distribution with the strain $\varepsilon$. Moreover, the values of the strain $\varepsilon$ and the damage variable $D$ at strain gauge 6 were much larger than the values at strain gauges 1 to 3. As it was expected, the closer to the bending neutral layer, the smaller the strain $\varepsilon$ and the damage variable $D$, the farther to the bending neutral layer, the larger the strain $\varepsilon$ and the damage variable $D$. This phenomenon was consistent with the actual situation of the test, indicating that the theoretical expression of the damage variable $D$ was reasonable.

*3.4. Verification and Discussion on Space-Time Evolution of the Bending Neutral Layer.* Substituting the parameters of Tables 1–3 into equation (20), the space-time evolution equation of the bending neutral layer can be derived as

$$y_0 = \frac{100 - \left(1 - \sqrt{1 - 1.72157 \times 10^{-10} \cdot e^{0.29t}}\right)}{2 + 2\sqrt{1 - 1.72157 \times 10^{-10} \cdot e^{0.29t}}}. \tag{22}$$

According to equation (22), we get the evolution curve of the bending neutral layer as shown in Figure 9. Figure 9 shows that the bending neutral layer moved slowly towards the compressive zone, a small distance in the range of 0 s–65 s, but moved fast a long distance in the range of 65 s–80 s. In correspondence to the experimental phenomena, there was no macrocrack propagation in the range of 0 s–65 s so that the position of the bending neutral layer was almost same as before. However, with

(a) (b) (c)

Figure 3: Stress-strain acquisition equipment and PCI-2 type acoustic emission system. (a) WAW-1000 kN microcomputer controlled electro-hydraulic servo universal testing machine; (b) DH3818 static strain data acquisition instrument; (c) the PCI-2 type acoustic emission system.

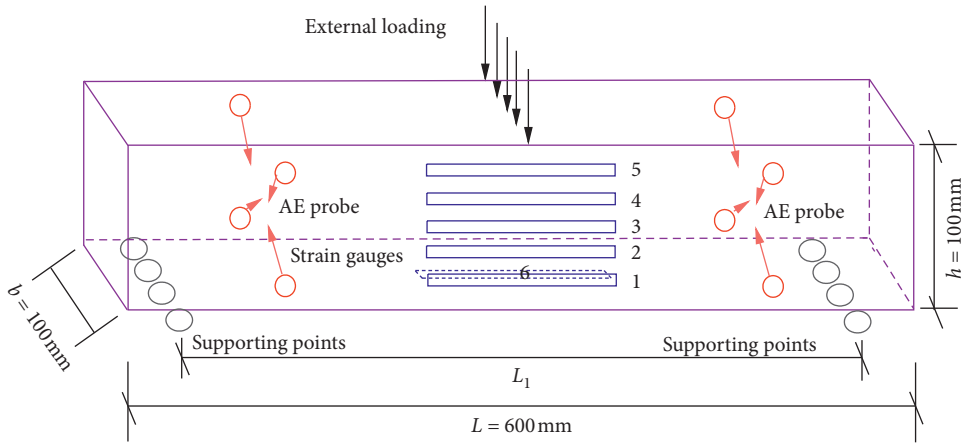


Figure 4: Three-point bending loading configuration and strain gauge layout.

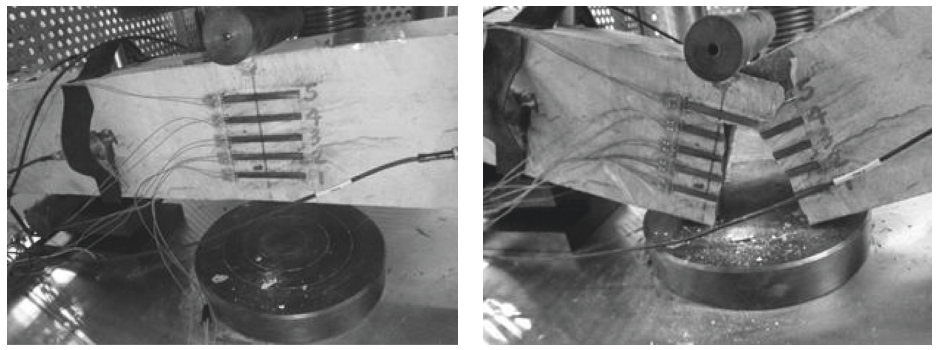

(a) (b)

Figure 5: (a) The installed limestone sample. (b) The fractured limestone sample.

the unstable macrocrack growth, the fractured portion of the limestone lost the ability of bearing bending deformation, which made redistribution of the bending neutral layer in undamaged portion of the limestone. Therefore, the bending neutral layer exhibited an obvious migration behavior in the range of 65 s–80 s. In short, the correlation between the theoretical curve analysis and the experimental phenomena verified the rationality of space-time evolution equation.

*3.5. Verification and Discussion of Bending Stress and Bending Strain.* The strain data are collected directly by the DH3818 static strain data acquisition instrument, and the stress data

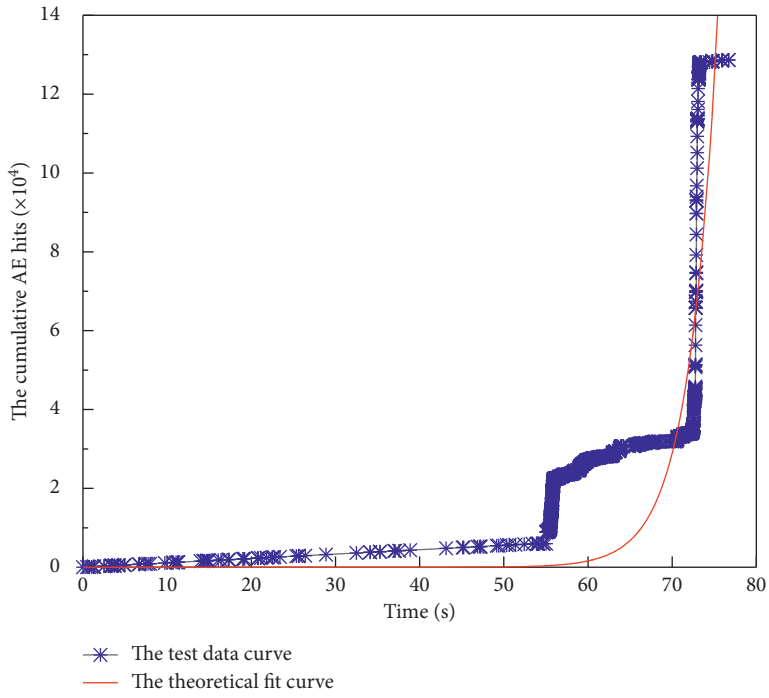


Figure 6: Relationship between the cumulative AE hits and time.

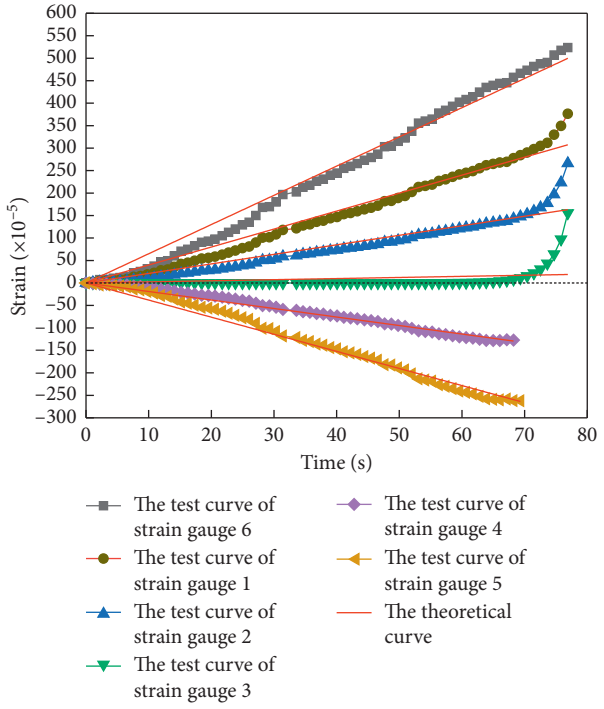


Figure 7: Relationship between the strain and time.

are acquired indirectly by equations (23)–(25) of material mechanics.

$$\sigma = \frac{M \cdot y}{I_z}, \tag{23}$$

$$M = \frac{P \cdot L}{4}, \tag{24}$$

$$I_z = \frac{b \cdot h^3}{12}, \tag{25}$$

where $M$ is the maximum bending moment, $P$ is the vertical compressive load, $L$ is the length of the limestone sample, $b$ is the width of section, $h$ is the height of section, $I_z$ is the moment of inertia of the cross section to the bending neutral

Table 1: Parameter fitting values of $A_1$, $B$, and $C$.

| | $N = A_1 \exp(Bt) + C$ | | |
|---|---|---|---|
| | $A_1$ | $B$ | $C$ |
| Parameter fitting values | $4.41 \times 10^{-5}$ | 0.29 | 0 |

Table 2: Parameter fitting values of $A_2$.

| Position of discussion | $\varepsilon = A_2 t$ $A_2$ |
|---|---|
| Strain gauge 1 | $3.99757 \times 10^{-5}$ |
| Strain gauge 2 | $2.12136 \times 10^{-5}$ |
| Strain gauge 3 | $0.24515 \times 10^{-5}$ |
| Strain gauge 4 | $-1.89343 \times 10^{-5}$ |
| Strain gauge 5 | $-3.804 \times 10^{-5}$ |
| Strain gauge 6 | $6.49918 \times 10^{-5}$ |

Table 3: Basic physical parameter values of the limestone.

| $L$ (mm) | $b$ (mm) | $h$ (mm) | $E$ (GPa) | $N_p$ | $\sigma_p$ (GPa) | $\varepsilon_p$ |
|---|---|---|---|---|---|---|
| 600 | 100 | 100 | 6.83 | 128655 | 0.01780 | $523.5 \times 10^{-5}$ |

Table 4: Equation of the damage variable with the strain.

| Position of discussion | Equation of the damage variable with the strain |
|---|---|
| Strain gauge 1 | $D = 1.72157 \times 10^{-10} \times e^{7254\varepsilon}$ |
| Strain gauge 2 | $D = 1.72157 \times 10^{-10} \times e^{13670\varepsilon}$ |
| Strain gauge 3 | $D = 1.72157 \times 10^{-10} \times e^{502861\varepsilon}$ |
| Strain gauge 6 | $D = 1.72157 \times 10^{-10} \times e^{4462\varepsilon}$ |

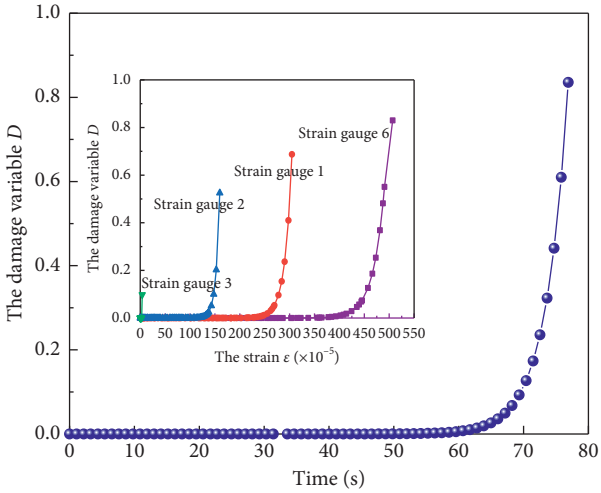


Figure 8: The evolution curves of the damage variable.

layer, and $y$ is the distance from the stress location to the bending neutral layer.

In this paper, the distance between strain gauges 1 to 6 and the initial bending neutral layer is 30 mm, 15 mm, 0 mm, −15 mm, −30 mm, and 50 mm, respectively. The corresponding $y$ values are shown in Table 5. Substituting the

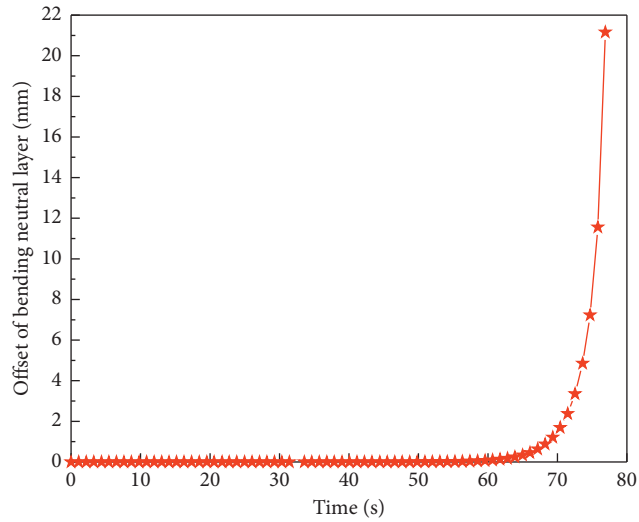


Figure 9: Relationship between the offset of bending neutral layer and time.

Table 5: The distance from the stress location to the bending neutral layer.

| Position of discussion | The corresponding $y$ values |
|---|---|
| Strain gauge 1 | $y = 30 + y_0$ |
| Strain gauge 2 | $y = 15 + y_0$ |
| Strain gauge 3 | $y = 0 + y_0$ |
| Strain gauge 4 | $y = -15 + y_0$ |
| Strain gauge 5 | $y = -30 + y_0$ |
| Strain gauge 6 | $y = 50 + y_0$ |

parameters of Tables 1–3 into equations (12)–(15), the stress evolution equation and the stress-strain constitutive relationship can be derived as in Table 6.

By the testing data collected by using experiment instruments of this paper, we get the relationship between the stress and time (Figure 10) as well as the relationship between the stress and the strain (Figure 11). Besides, using the testing data of strain gauge 6 to verify the theory models, the comparison curve between the test and the theory model about relationship of $\sigma$, $t$ is shown in Figure 12, the comparison curve between the test and the theory model about relationship of $\sigma$, $\varepsilon$ is shown in Figure 13.

In Figure 10, the stress exhibited a slow-growth behavior due to a smaller vertical compressive load in the range of 0 s–10 s, accompanying crack closing of the limestone sample. With continuous increasing of the vertical compressive load, the stress grew stably with testing time in the range of 10 s–65 s, showing elastic properties of the limestone sample. Up to ultimate bending bearing capacity, the macrocrack propagated from the tensile zone to the compressive zone and the stress grew unstably with testing time in the range of 65 s–80 s. More importantly, Figure 10 also shows a nonuniform distribution of the stress in the bending process, and the farther the bending neutral layer, the larger the stress.

Figure 11 shows the same nonuniform distribution of the stress and the strain, too. For example, the stress and

Table 6: The distance from the stress location to the bending neutral layer.

| Position | The stress evolution equation | The stress-strain constitutive relationship |
|---|---|---|
| Strain gauge 1 | $\sigma_{t_{(1)}} = 0.27303 \cdot t - 4.7004 \times 10^{-11} \cdot t \cdot e^{0.29t}$ | $\sigma_{t_{(1)}} = 0.0683 \cdot \varepsilon - 1.1758 \times 10^{-11} \cdot \varepsilon \cdot e^{7254\varepsilon}$ |
| Strain gauge 2 | $\sigma_{t_{(2)}} = 0.14489 \cdot t - 2.4944 \times 10^{-11} \cdot t \cdot e^{0.29t}$ | $\sigma_{t_{(2)}} = 0.0683 \cdot \varepsilon - 1.1758 \times 10^{-11} \cdot \varepsilon \cdot e^{13670\varepsilon}$ |
| Strain gauge 3 | $\sigma_{t_{(3)}} = 0.00394 \cdot t - 6.78103 \times 10^{-13} \cdot t \cdot e^{0.29t}$ | $\sigma_{t_{(3)}} = 0.0683 \cdot \varepsilon - 1.1758 \times 10^{-11} \cdot \varepsilon \cdot e^{502861\varepsilon}$ |
| Strain gauge 4 | $\sigma_{c_{(4)}} = -0.12932 \cdot t$ | $\sigma_{c_{(4)}} = 0.0683 \cdot \varepsilon$ |
| Strain gauge 5 | $\sigma_{c_{(5)}} = -0.21064 \cdot t$ | $\sigma_{c_{(5)}} = 0.0683 \cdot \varepsilon$ |
| Strain gauge 6 | $\sigma_{t_{(6)}} = 0.44389 \cdot t - 4.76419 \times 10^{-11} \cdot t \cdot e^{0.29t}$ | $\sigma_{t_{(6)}} = 0.0683 \cdot \varepsilon - 1.1758 \times 10^{-11} \cdot \varepsilon \cdot e^{4462\varepsilon}$ |

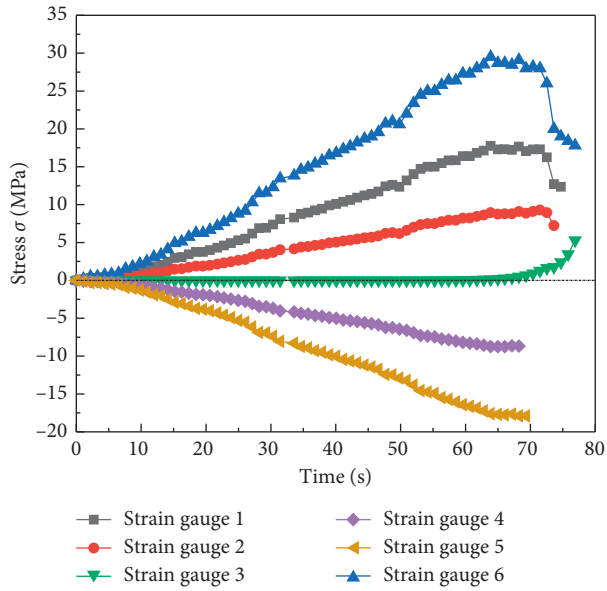


Figure 10: Relationship between the stress and time.

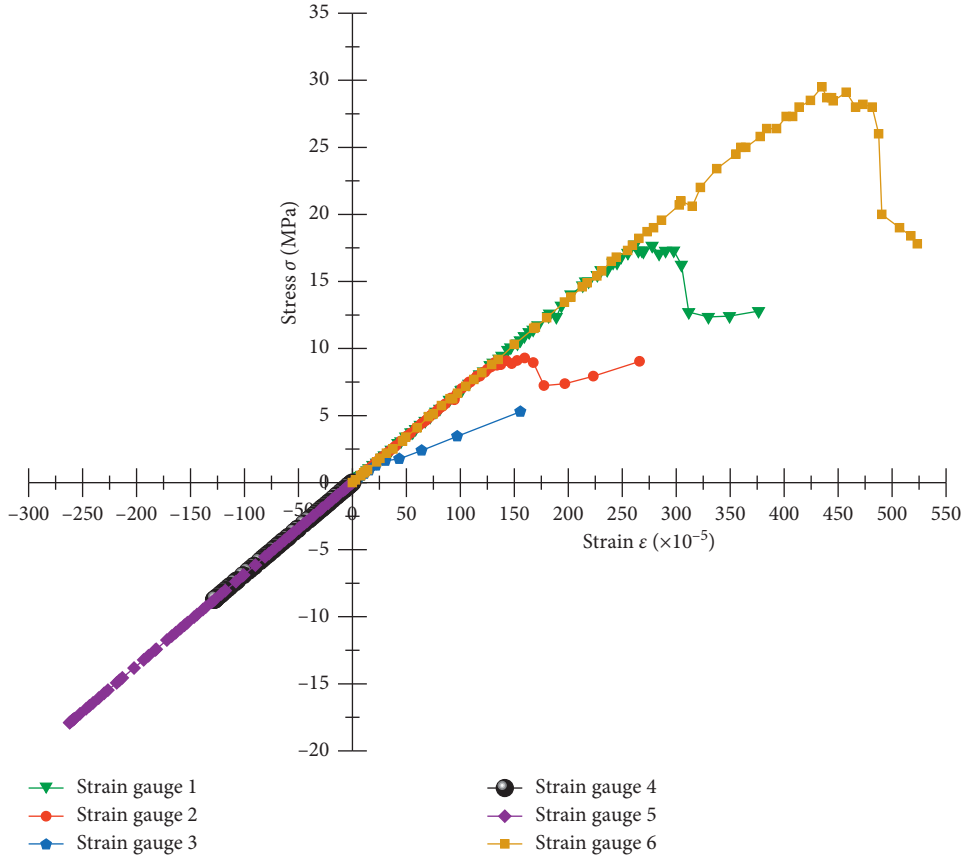


Figure 11: Relationship between the stress and the strain.

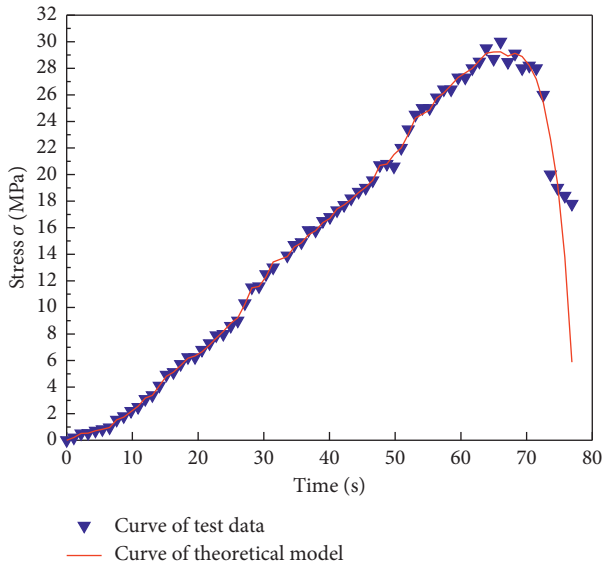


Figure 12: Comparison between test and model about relationship of $\sigma$, $t$ at strain gauge 6.

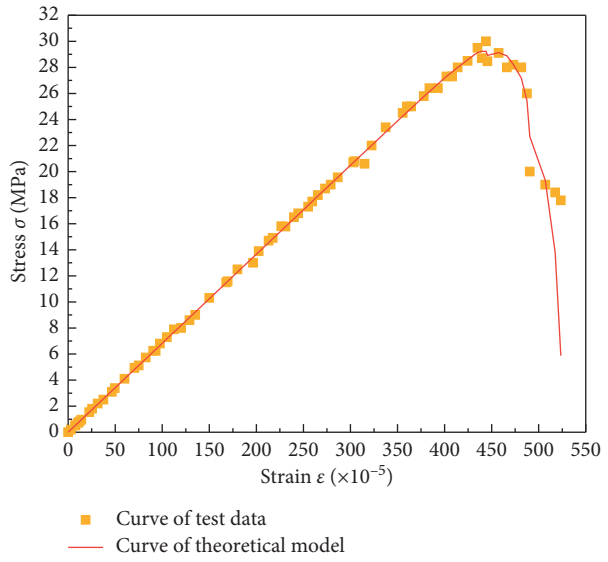


Figure 13: Comparison between test and model about relationship of $\sigma$, $\varepsilon$ at strain gauge 6.

the strain at strain gauge 6 were much larger than the stress and the strain at strain gauge 1. Besides, the phenomena that the bending tensile stress yield decreased and the bending compressive stress still increased linearly indicated that the ultimate tensile strength of limestone is much lower than the ultimate compressive strength.

In Figures 12 and 13, there was a good match between the curves of test data and the curves of theoretical model. This showed that the theoretical model curves agreed with the testing process, and the proposed model reflected the damage evolution of limestone reasonably in the bending damage process.

## 4. Conclusions

In this paper, the characteristics and constitutive model of limestone in the bending damage process were studied, and the three-point bending test with AE monitoring was carried out to verify the proposed model. The following conclusions were drawn:

(1) The prevailing damage variable equation defined by AE hits was developed, and the modified damage variable $D$ had an exponential distribution with the strain $\varepsilon$, which agreed with the testing process more.

(2) The quantitative space-time evolution equation of the bending neutral layer in the bending process was built. The bending neutral layer moved slowly at the initial stage of bending fracture but moved fast at the end stage of bending fracture.

(3) The bending damage stress-strain constitutive model was derived. And it could be quantitatively expressed by the cumulative AE hits $N_p$, the stress $\sigma$, the strain $\varepsilon$, and Young's modulus $E$.

(4) The three-point bending test with AE monitoring was conducted to verify the rationality and validity of the proposed model. As it was expected, curves from the proposed model agreed very well with the testing data, which indicated that the model was effective to characterize the bending damage process of limestone.

## Data Availability

The data used to support the findings of this study are available from the corresponding author upon request.

## Conflicts of Interest

The authors declare that there are no conflicts of interest regarding the publication of this paper.

## Acknowledgments

The authors gratefully acknowledge the support of the National Natural Science Foundation of China (grant no. 406 51469007), First Class Subject Foundation of Civil Engineering of Guizhou Province (QYNYL[2017]0013), Mountain Geohazard Prevention R&D Center of Guizhou Province ([2017]5402), and Guizhou Science and Technology Support Project for Social Development ([2017]2866).

## References

[1] Z. Y. Liao, J. B. Zhu, and C. A. Tang, "Numerical investigation of rock tensile strength determined by direct tension, Brazilian and three-point bending tests," *International Journal of Rock Mechanics and Mining Sciences*, vol. 115, pp. 21–32, 2019.

[2] M. Cai, P. K. Kaiser, and C. D. Martin, "Quantification of rock mass damage in underground excavations from microseismic event monitoring," *International Journal of Rock Mechanics and Mining Sciences*, vol. 38, no. 8, pp. 1135–1145, 2001.

[3] L. C. Li, C. A. Tang, W. C. Zhu, and Z. Z. Liang, "Numerical analysis of slope stability based on the gravity increase method," *Computers and Geotechnics*, vol. 36, no. 7, pp. 1246–1258, 2009.

[4] R. J. Pine, D. R. J. Owen, J. S. Coggan, and J. M. Rance, "A new discrete fracture modelling approach for rock masses," *Géotechnique*, vol. 57, no. 9, pp. 757–766, 2007.

[5] G. E. Andreev, "A review of the Brazilian test for rock tensile strength determination. Part I: calculation formula," *Mining Science and Technology*, vol. 13, no. 3, pp. 445–456, 1991.

[6] Z. Zhang, *Principles of Engineering Geology*, Geologic Press, Beijing, China, 2nd edition, 1994.

[7] G. Sun, *Mechanics of Rock Mass Structures*, Science Press, Beijing, China, 1988.

[8] G. Barla and N. Innaurato, "Indirect tensile testing of anisotropic rocks," *Rock Mechanics and Rock Engineering*, vol. 5, no. 4, pp. 215–230, 1973.

[9] ASTM International, *Standard Test Method for Splitting Tensile Strength of Intact Rock Core Specimens*, ASTM International, West Conshohocken, PA, USA, 2008.

[10] International Society for Rock Mechanics, "Suggested methods for determining tensile strength of rock materials," *International Journal of Rock Mechanics and Mining Sciences &, Geomechanics Abstracts*, vol. 15, no. 3, pp. 99–103, 1978.

[11] P. Pandey and D. P. Singh, "Deformation of a rock in different tensile tests," *Engineering Geology*, vol. 22, no. 3, pp. 281–292, 1986.

[12] X.-p. Zhang, Q. Zhang, and S. Wu, "Acoustic emission characteristics of the rock-like material containing a single flaw under different compressive loading rates," *Computers and Geotechnics*, vol. 83, pp. 83–97, 2017.

[13] E. J. Kaiser, *A Study of Acoustic Phenomena in Tensile Test*, Technical University of Munich, Munich, Germany, 1950.

[14] D. Lockner, "The role of acoustic emission in the study of rock fracture," *International Journal of Rock Mechanics and Mining Sciences & Geomechanics Abstracts*, vol. 30, no. 7, pp. 883–899, 1993.

[15] W. Yao, K. Xia, and A. K. Jha, "Experimental study of dynamic bending failure of Laurentian granite: loading rate and pre-load effects," *Canadian Geotechnical Journal*, vol. 56, no. 2, pp. 228–235, 2019.

[16] P. R. Prem and A. R. Murthy, "Acoustic emission monitoring of reinforced concrete beams subjected to four-pointbending," *Applied Acoustics*, vol. 117, pp. 28–38, 2016.

[17] G. Lacidogna, G. Piana, and A. Carpinteri, "Acoustic emission and modal frequency variation in concrete specimens under four-point bending," *Applied Sciences*, vol. 7, no. 4, p. 339, 2017.

[18] Y. Lu, W. Li, L. Wang et al., "In-situ microscale visualization experiments on microcracking and microdeformation behaviour around a pre-crack tip in a three-point bending sandstone," *International Journal of Rock Mechanics and Mining Sciences*, vol. 114, pp. 175–185, 2019.

[19] K. Kaklis, S. Maurigiannakis, Z. Agioutantis, and C. Istantso, "Influence of specimen shape on the indirect tensile strength of transversely isotropic Dionysos marble using the three-point bending test," *Strain*, vol. 45, no. 5, pp. 393–399, 2009.

[20] H. Zhang, D. Fu, H. Song et al., "Damage and fracture investigation of three-point bending notched sandstone beams by DIC and AE techniques," *Rock Mechanics and Rock Engineering*, vol. 48, no. 3, pp. 1297–1303, 2015.

[21] W. Yao, K. W. Xia, and X. Li, "Non-local failure theory and two-parameter tensile strength model for semi-circular bending tests of granitic rocks," *International Journal of Rock Mechanics and Mining Sciences*, vol. 110, pp. 9–18, 2018.

[22] W. G. Rong, M. D. Yao, J. Peng, S. Sha, and J. Tan, "Influence of initial thermal cracking on physical and mechanical behaviour of a coarse marble: insights from uniaxial compression tests with acoustic emission monitoring," *Geophysical Journal International*, vol. 214, no. 3, pp. 1886–1900, 2018.

[23] Y. Chen, Y. G. Yang, F. Gao, and X. Zhang, "Researches on damage evolution and acoustic emission characteristics of rocks," *Advances In Civil Engineering*, vol. 2018, Article ID 3108065, 7 pages, 2018.

[24] P. Jin, E. Wang, and D. Song, "Study on correlation of acoustic emission and plastic strain based on coal-rock damage theory," *Geomechanics and Engineering*, vol. 12, no. 4, pp. 627–637, 2017.

[25] J. Xu, C. Zhai, P. G. Ranjith, Y. Sun, and L. Qin, "Petrological and ultrasonic velocity changes of coals caused by thermal cycling of liquid carbon dioxide in coalbed methane recovery," *Fuel*, vol. 249, pp. 15–26, 2019.

[26] G. Lacidogna, G. Piana, and A. Carpinteri, "Damage monitoring of three-point bending concrete specimens by acoustic emission and resonant frequency analysis," *Engineering Fracture Mechanics*, vol. 210, pp. 203–211, 2019.

[27] A. Cazzani, M. Malagù, E. Turco, and F. Stochino, "Constitutive models for strongly curved beams in the frame of isogeometric analysis," *Mathematics and Mechanics of Solids*, vol. 21, no. 2, pp. 182–209, 2016.

[28] X. Li, W.-G. Cao, and Y.-H. Su, "A statistical damage constitutive model for softening behavior of rocks," *Engineering Geology*, vol. 143-144, pp. 1–17, 2012.

[29] J. Lemaitre and J. L. Chaboche, *Mechanics of Solid Materials*, Cambridge University Press, Cambridge, UK, 1990.

[30] J. Lemaitre, "How to use damage mechanics," *Nuclear Engineering and Design*, vol. 80, no. 2, pp. 233–245, 1984.

[31] C. A. Tang and X. H. Xu, "Evolution and propagation of material defects and kaiser effect function," *Journal of Seismological Research*, vol. 13, no. 2, pp. 203–213, 1990.

[32] X. Z. Wu, J. W. Liu, X. X. Liu et al., "Study on the coupled relationship between AE accumulative ring-down count and damage constitutive model of rock," *Caikuang Yu Anquan Gongcheng Xuebao/Journal of Mining and Safety Engineering*, vol. 32, no. 1, pp. 28–35, 2015, in Chinese.

[33] T. F. Wong, H. C. W. Robina, K. T. Chau, and C. A. Tang, "Microcrack statistics, Weibull distribution and micromechanical modeling of compressive failure in rock," *Mechanics of Materials*, vol. 38, no. 7, pp. 664–681, 2006.

[34] J. Deng and D. Gu, "On a statistical damage constitutive model for rock materials," *Computers & Geosciences*, vol. 37, no. 2, pp. 122–128, 2011.

[35] D. N. Pazis, N. P. Andrianopoulos, I. Vardoulakis et al., "Bending of Dionysos marble architraves," in *Proceedings of the International Symposium on Geotechnical Engineering for the Preservation of Monuments and Historical Sites*, pp. 251–260, Balkema, Napoli, Italy, 1996.

[36] S. K. Kourkoulis, Z. Agioutantis, S. Maurigiannakis, and E. Papatheodorou, "Experimental and numerical analysis of notched marble beams under bending: an elastic transversely isotropic model," in *Proceedings of the International Conference on Computational & Experimental Engineering & Sciences*, Corfu, Greece, July 2003.

[37] G. E. Exadaktylos and S. K. Kourkoulis, "Three-point bending of transversely isotropic rock-type materials: an analytical, numerical and experimental study," in *Proceedings of the 4th Greek Association of Computational Mechanics Congress on Computational Mechanics*, Patras, Greece, June 2002.

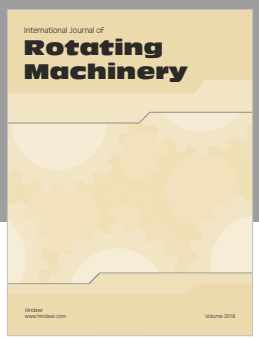

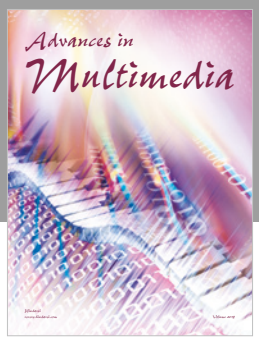

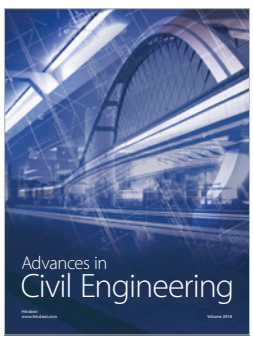

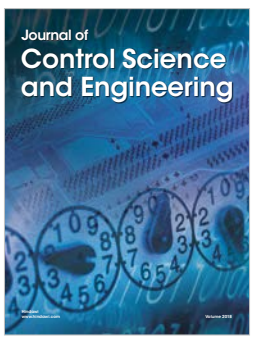

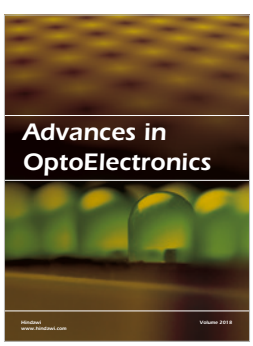

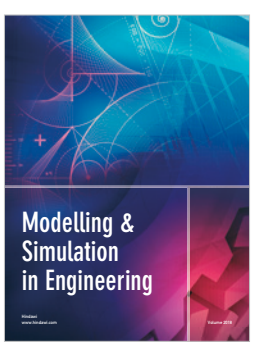

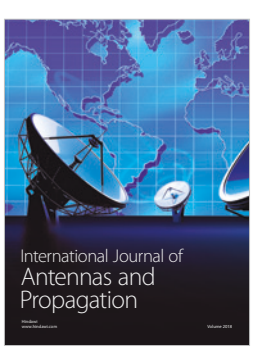

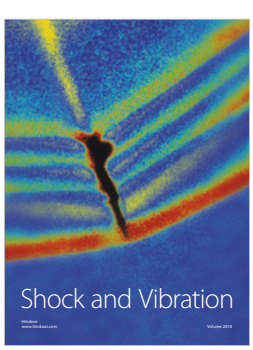

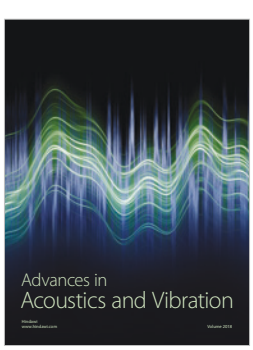

Hindawi

Submit your manuscripts at
www.hindawi.com